Chemosphere xxx (xxxx) 135233

Contents lists available at ScienceDirect

Chemosphere

journal homepage: www.elsevier.com/locate/chemosphere

Fabrication and characterization of a novel Ba^{2+}-loaded sawdust biochar doped with iron oxide for the super-adsorption of SO_4^{2-} from wastewater

Warda Khalid [a], Chin Kui Cheng [b], Peng Liu [a,*], Jinping Tang [a], Xin Liu [a], Asmat Ali [a], Asfandyar Shahab [c], Xingjie Wang [a]

[a] School of Environmental Studies & State Key Laboratory of Biogeology and Environmental Geology, China University of Geosciences, Wuhan, 430074, China
[b] Center for Catalysis and Separation, Department of Chemical Engineering, College of Engineering, Khalifa University of Science and Technology, P. O. Box 127788, Abu Dhabi, United Arab Emirates
[c] College of Environmental Science and Engineering, Guilin University of Technology, Guilin, 541004, China

ARTICLE INFO

Handling editor: Derek Muir.

Keywords:
Wastewater treatment
Sulfate removal
Activated biochar
Adsorption kinetics
Chemisorption

ABSTRACT

Biochar is a low-cost adsorbent used in the treatment of contaminated wastewater. We investigated the potential of an Fe-impregnated, Ba^{2+}-loaded biochar (Fe-(Ba-BC)) for the removal of SO_4^{2-} from aqueous solutions. The Ba^{2+}-loaded biochar was synthesized from sawdust impregnated with iron oxide via pyrolysis at 600 °C. The porous structure of the Fe-(Ba-BC) was identified by scanning electron microscopy before sulfate was adsorbed onto the adsorbent. Functional groups were determined by energy-dispersive spectrophotometry and Raman spectrometry.. The Fe-(Ba-BC) Raman peaks before the experiment were higher than after, suggesting the precipitation of $BaSO_4$. The presence of $BaCl_2$ on the surface of the biochar was confirmed by X-ray diffraction. Batch sorption results showed that Fe-(Ba-BC) strongly adsorbed aqueous SO_4^{2-} with a removal efficacy of 96.7% under the optimum conditions of 0.25 M $BaCl_2$, a contact time of 480 min, a pH of 9 and an adsorbent dose of 2 g. The optimum condition for removal and reaction rate kinetics analysis indicated that adsorption curve fitted well with PSO, k_2 0.00015 confirmed the removal of SO_4^{2-} via chemisorption. Thus, Fe-(Ba-BC) was found to be a favorable adsorbent for removing SO_4^{2-}.

1. Introduction

Sulfate (SO_4^{2-}), the anion of sulfuric acid (H_2SO_4), is released into the natural environment as a consequence of both human activities (e.g., mining, livestock farming, food production, paper milling, and chemical and detergent manufacturing) and natural phenomena (e.g., geological processes such as the eruption of volcanoes) (Zak et al., 2021). High concentrations of SO_4^{2-} in wastewater pose severe threats to aquatic ecosystems and contribute to the formation of acid rain, corrosion and the release of toxic gases into the atmosphere (Dutta et al., 2010). High concentrations of SO_4^{2-} in potable water supplies cause diarrhea, dehydration, a laxative effect and gastric upset in humans (Bashir et al., 2012). The World Health Organization and the United States Environmental Protection Agency (EPA) have set a limit of 250 mg L^{-1} SO_4^{2-} for drinking water (EPA, 2017; Water and Organization, 2006), although concentrations >400 mg L^{-1} have been reported in wastewater by (Chen et al., 2020). The removal of SO_4^{2-} from effluents has attracted much attention in recent years as a result of its harmful consequences (Mohammadi et al., 2019). Stringent standards for SO_4^{2-} in water will force many water service providers to improve traditional treatment systems or to seek alternative purification technologies (Silva et al., 2020).

Various conventional treatments have been used to remove SO_4^{2-} from wastewater, including reverse osmosis, chemical precipitation, flotation, membrane filtration (Al-Zoubi et al., 2007), ion exchange (Tang et al., 2017) and electrocoagulation (Rodrigues et al., 2020). Adsorption has been shown to be the most viable and economic technique for the removal of SO_4^{2-} (Yi et al., 2020), particularly in developing countries. A number of different adsorbents have been investigated, including functionalized carbon nanotubes (Li et al., 2014), nanocomposites (Mo et al., 2021, 2022), biosorbents (Lu et al., 2021; Wang and Chen, 2014), plant biomass (Alvarez et al., 2015; Zeng et al., 2021) and kaolin (Hudaib, 2021). Sawdust and bamboo being economical and is easily available which can be acquired locally. Sawdust biochar has been shown to be one of the most promising and economic adsorbents.

* Corresponding author.
E-mail address: pengliu@cug.edu.cn (P. Liu).

https://doi.org/10.1016/j.chemosphere.2022.135233
Received 12 April 2022; Received in revised form 25 May 2022; Accepted 2 June 2022
0045-6535/

Organic and inorganic compounds have been used to modify biochar to improve the adsorption capacity (Srivatsav et al., 2020).

Biochar is a low-cost adsorbent generated via the pyrolysis of biomass and waste products in an oxygen-deficient environment (Sun et al., 2019) and is an excellent candidate for the removal of inorganic pollutants (e.g., SO_4^{2-}). Biochar is suitable for the removal of a wide range of pollutants as a result of its high availability, large surface area, low cost and excellent bio-absorption via the development of pore structures (Liang et al., 2021).

Biochar can be modified via physical, chemical, magnetic and impregnation methods to increase adsorption and can be modified to change its selectivity (Rajapaksha et al., 2016). Magnetic biochar can be prepared by impregnating the biomass with iron oxide via pyrolysis (Chen et al., 2011). Various types of modified biochar have been used to remove sulfate from water, including pomelo peel biochar modified with zirconium oxide (Ao et al., 2020), Fe-modified carbon residues (Runtti et al., 2016) and modified sugarcane bagasse cellulose (Mulinari & da Silva, 2008). Earlier studies (Cheng et al., 2012) used magnetic Fe_3O_4 particle modified sawdust for the removal of strontium ions with a total 12.59 mg g^{-1}adsorption capacity, while (Feng et al., 2019) used magnetic natural composite Fe_3O_4-chitosan@bentonite for the removal of heavy metal following maximum adsorption capacity of 62.1 mg g^{-1}. However, the simultaneous modification of biochar impregnated with Ba^{2+} and magnetization with Fe has not been reported previously.

This study evaluated Fe-impregnated biochar sawdust loaded with Ba^{2+} from $BaCl_2$ via pyrolysis for the removal of SO_4^{2-} from wastewater. Fe-impregnated biochar enhances the removal of pollutants because it increases the surface area of the biochar, is more reactive in water and can donate protons (Liang et al., 2021). Biochar may have more surface O-containing functional groups (e.g., C–O, C–O–C and C═O) than carbon, which can interact with Fe to produce multi-functional Fe–biochar complexes (Wang et al., 2022).

This study explored the effectiveness of Fe-impregnated, Ba^{2+}-loaded adsorbents for the removal of SO_4^{2-} through adsorption-assisted precipitation. The effects of the contact time, pH, molar concentration of Ba^{2+}, adsorbent and adsorbate dose were evaluated in a 1500 mg L^{-1} solution of SO_4^{2-} at 22 ± 2 °C in order to remove the maximum concentration of sulfate levels (>1500 mg L^{-1}) in industrial effluents. This maximum removal of sulfate has rarely been reported in other related studies which makes it an innovative aspect of this study. Various adsorption kinetic models were investigated to determine the mechanism of the adsorption-assisted precipitation process.

2. Materials and methods

A CAS No. KB05670 standard solution of sulfate (SO_4^{2-}) was obtained from Beijing Wanjia Shouhua Biological Technology Co. Ltd. All reagents used in the experiments were of high purity. Deionized water was used to prepare all the chemical solutions and to rinse and clean the samples. Solutions of NaOH (98%), HCl (95–99%), $Na_2SO_4^{2-}$ (99.5%), $BaCl_2$ (99%) and $NaNO_3$ (>99.5%) were purchased from Merck (Germany) and used as supplied.

2.1. Preparation of Fe-impregnated Ba^{2+}-loaded biochar

Biochar was prepared using sawdust as the raw biomass and was magnetized by the addition of iron oxide Fe-(Ba-BC) via chemical co-precipitation (Gillingham et al., 2021) followed by pyrolysis at 600 °C. The raw materials were dried in an oven for 24 h at 45 °C. $BaCl_2$ was impregnated via chemical activation by placing the absorbent in a 0.1 M solution of $BaCl_2$ for 4 h, followed by drying in an oven for 24 h at 45 °C. The Fe-(Ba-BC) was placed in a muffle furnace for 4 h at 600 °C under a flow of N_2 gas to convert raw biomass into biochar. The prepared Fe-(Ba-BC) was stored in polyethylene bags (Li et al., 2019).

Using the same process, various biochar samples were prepared using different materials and with different concentrations of iron oxide: sawdust fine (SDF); sawdust + FeO 12.5 g (SD1); sawdust + FeO 25 g (SD2); bamboo fine + FeO 12.5 g (BBF1); bamboo fine + FeO 50 g (BBF2); bamboo coarse + FeO 50 g (BBC); bamboo rough + FeO 12.5 g (BBR1); bamboo rough + FeO 25 g (BBR2); and two bamboo scraps (BBS1 and BBS2) (Table 1).

2.2. Characterization of Fe-impregnated Ba^{2+}-loaded biochar

The surface morphology of the Fe-(Ba-BC) samples was examined by scanning electron microscopy (SEM) (TESCAN VEGA3) at 20 kV with energy-dispersive X-ray spectrometry (EDS; Oxford AZtecOne XT) at 10 kV. Samples of Fe-(Ba-BC) before and after reaction were prepared on carbon tape and imaged under different magnifications at a working distance of 14.96 mm. Raman spectra were recorded in the range 500–4000 cm^{-1} before and after the experiment (Asadullah et al., 2010). X-ray diffraction (XRD) was performed using an X'Pert PRO Dy98 instrument at 5° min^{-1} and a peak deconvolution method was applied to investigate the data (Park et al., 2010). The built-in Gaussian functions in Origin Pro (2021b) were used to match the peaks (Zhang et al., 2014). Samples obtained before and after the optimized experiment were packed into polyethylene bags before being transferred to the laboratory for characterization.

2.3. Adsorption and precipitation activity

2.3.1. Preparation of sulfate solutions

A 1500 mg L^{-1} SO_4^{2-} stock solution was prepared and used to derive standard solutions of 5, 10, 15, 20, 25, 30, 35 and 40 mg L^{-1} SO_4^{2-}. The standard curve was determined at a wavelength of 450 nm. The optimum wavelength of 450 nm has been selected for the sulfate removal due to the maximum absorbance by sulfate.

2.3.2. Analytical procedures

The pH was measured using a digital pH meter (PHS–38W Microprocessor). A digital furnace (DRPT Co. Ltd) was used for sawdust pyrolysis. An oven (DHG-9101 Wincom Co. Ltd) was used to dry the samples and a rolling incubator (Haimen Kylin-Bell Instruments Co. Ltd) was used to mix them. A plastic syringe filter (pore size 0.45 μm) was used to filter the samples. The absorbance of the supernatant was measured at 450 nm using a GENESYS 50 UV–visible spectrophotometer.

2.3.3. Experimental procedures

Adsorption-assisted precipitation experiments were conducted to determine the efficacy of the modified biochars for the removal of SO_4^{2-} from wastewater. The experiments were performed in a 50 mL centrifuge tube using a 1500 mg L^{-1} solution of SO_4^{2-} (40 mL working volume) to optimize various parameters. NaOH (0.1 M) and HCl (0.1 M) were used to adjust the initial pH of the sample. Batch adsorption and precipitation experiments were carried out using a known

Table 1
Composition of biochar samples.

Sample	Type of biochar	FeO (g)
SDF	Sawdust, fine	–
SD1	Sawdust	12.5
SD2	Sawdust	25
BBF1	Bamboo, fine	12.5
BBF2	Bamboo, fine	50
BBC	Bamboo, coarse	50
BBR1	Bamboo, rough	12.5
BBR2	Bamboo, rough	25
BBS1	Bamboo, scraps	–
BBS2	Bamboo, scraps	–

amount of modified Fe-(Ba-BC) in 40 mL of a 1500 mg L^{-1} SO_4^{2-} solution mixed at 220 rpm on a rotatory machine at room temperature. After the optimized contact time, the samples were filtered through a 0.45-μm syringe filter and the concentration of SO_4^{2-} remaining measured by spectrophotometry.

The effect of various parameters affecting precipitation-assisted adsorption were optimized at a constant concentration of 1500 mg L^{-1}: pH (2–11), contact time (30–510 min), dose of adsorbent (0.5–5 g) and molar concentration of $BaCl_2$ (0.05–0.25 M). The optimized parameters used in the initial experiment to identify the most efficient modified biochar Fe-(Ba-BC) for adsorption-assisted precipitation in a working volume of 40 mL were: SO_4^{2-}, 1500 mg L^{-1}; pH, 5.70; dose of adsorbent, 0.5 g; contact time, 24 h; $BaCl_2$ concentration, 0.1 M; temperature 22 ± 2 °C; and speed of rotory mixing, 220 rpm. The supernatants were evaluated for absorbance at 450 nm using UV–visible spectrophotometry. All the experiments for adsorption-assisted precipitation were conducted in duplicate with a method blank to determine the accuracy of the results.

The concentration of SO_4^{2-} removed was determined by:

$$\text{Removal efficiency}(\%) = \frac{1 - C_f}{C_i} \times 100 \quad (1)$$

where C_i is the initial concentration of SO_4^{-2} (mg L^{-1}) and C_f is the final concentration. The duplicate efficacy of the samples was calculated using Eqs. (2) and (3):

$$d = X_1 - X_2 \quad (2)$$

$$(d)_r = \frac{d}{(X_1 + X_2)/2} \times 100 \quad (3)$$

where X_1 = concentration of sample 1 and X_2 = concentration of duplicate of sample 1.

2.4. Statistical analysis

Origin version 2021 software and Microsoft Excel for Windows 10 were used for the statistical analyses. The experiment was performed in duplicate and the mean values used in further analysis. The data are presented as the mean ± SD efficiency (%) of the removal of SO_4^{2-}.

2.5. Kinetics study

A number of different kinetic models have been used to determine the efficiency and mechanisms of adsorption of various chemicals. Most adsorption kinetic studies use pre-existing models as a guide to illustrate the adsorption mechanism. Kinetic models were used to investigate the adsorption system of Fe-(Ba-BC) for the removal of sulfate. The pseudo-first-order rate equation (Ho and McKay, 1998),intraparticle diffusion model (Lagergren, 1898), Elovich model (Zeldowitsch, 1934) waere used to consider the effects of time on adsorption.

3. Results and discussion

3.1. Characterization of Fe-(Ba-BC)

3.1.1. XRD studies

XRD was used to investigate the structure and phase purity of the Fe-(Ba-BC) samples (Fig. 1a). The biochar matrix with iron oxide had strong, sharp XRD peaks, indicating a high degree of crystallization. The XRD patterns of the Ba-BC samples before and after the experiment showed the highest reflection at $2\theta = 5.73°$. $BaSO_4$ peaks were present after the experiment, with the highest reflection at $2\theta = 4.45°$. Fig. 1a shows the analysis before $BaCl_2$ was loaded onto the Fe-(Ba-BC) and therefore the Ba^{2+} reflections are at their highest. The spectra show that Fe was present as hematite (Fe_2O_3), as reported previously by (Duan et al., 2017), and that 12.5 g of iron oxide had been added to the Fe-(Ba-BC). Reflections of $BaSO_4^{2-}$ were seen after the addition of Ba^{2+}, suggesting that the $BaCl_2$ successfully reacted with Na_2SO_4 to remove the SO_4^{2-} as a precipitate of $BaSO_4$.

3.1.2. Raman spectroscopy

Raman spectra were used to verify the graphitization process. Fig. 1b shows that the spectra of Fe-(Ba-BC) before and after the experiment were similar, with characteristic peaks at 1250 and 1550 cm^{-1} showing D (disordered graphitic carbon) and G (sp^2-hybridized graphitic carbon) bands, as reported by (Feng et al., 2016; Li et al., 2020). The intense Raman peaks between 500 and 4000 cm^{-1} showed that the electron-rich structures (e.g., O-containing functional groups) had high Raman scattering abilities, enhancing the observed Raman intensity (Tay et al., 2013). The Fe-(Ba-BC) peaks before the experiment were higher than those after the experiment, indicating the precipitation of $BaSO_4$. The intensity of the D and G bands of Fe-(Ba-BC) decreased as a result of heating, as reported previously by (Zheng and Dahn, 1999). At the same time, the formation of the peaks of both Fe-(Ba-BC) were related to each other.

3.1.3. SEM and EDS analysis

Five spots of each before and after the experiments, total 59 spectrums, were seen for EDS studies to support our findings with better spectra. Fig. 2a shows the EDS and SEM maps of Fe-(Ba-BC), illustrating the smooth surface and pore capacity of the Fe-(Ba-BC) samples. After modification, the Fe-(Ba-BC) surface became rough, with attached particles and pore structures filled with sulfate. The field view at a depth of 116 μm showed the highest Ba peaks (weight percentage 19.46 and

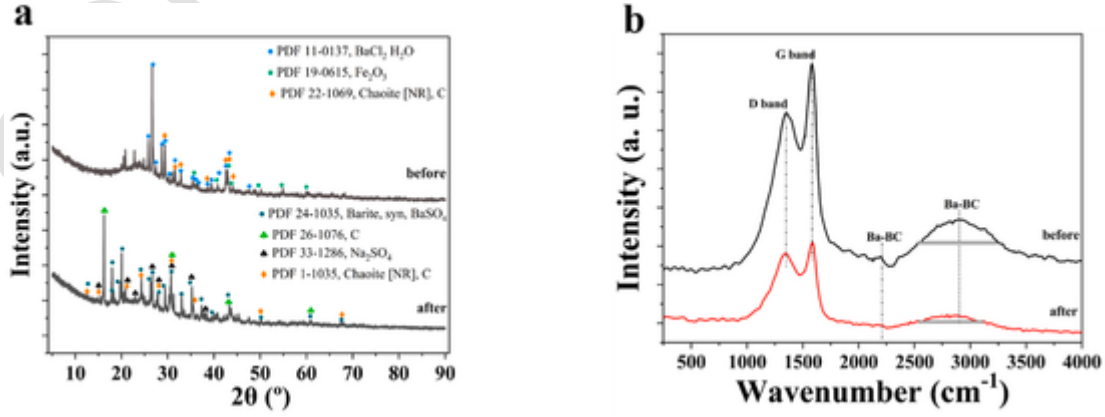

Fig. 1. X-ray diffraction (XRD) and Raman spectroscopy characterization of Fe-doped sawdust biochar before and after experiment. (**a**) XRD spectra; (**b**) Raman spectra showing D and G bands.

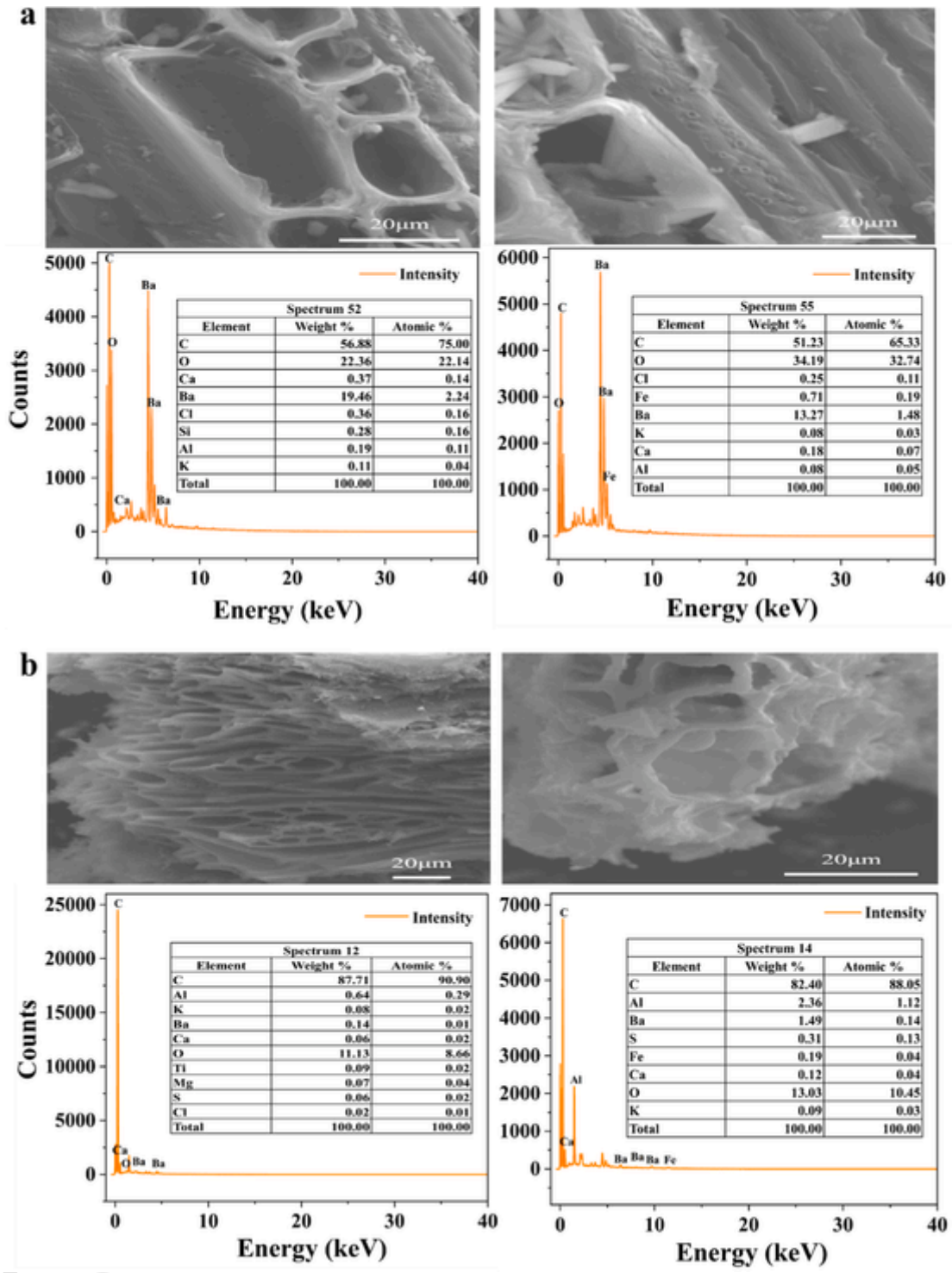

Fig. 2. Result of EDS-SEM analysis. (**a**) EDS spectra and SEM images of modified Fe-(Ba-BC) substrate before reaction with SO_4^{2-}; (**b**) EDS spectra and SEM images of modified Fe-(Ba-BC) substrate after reaction with SO_4^{2-}.

13.278%), evidence that $BaCl_2$ had been successfully loaded onto the Fe-(Ba-BC) samples. Apparent peaks of C and O were also visible. Peaks of metallic Au can be seen as a result of the coating added before the analysis to obtain high-resolution images.

After the experiment, Fe-(Ba-BC) showed the morphology of Fe-impregnated biochar with different decline peaks of Ba (weight percentage 0.14%) (Fig. 2b). Sulfur (0.11%) can also be seen, confirming that Ba was successfully precipitated as $BaSO_4$. Fig. 2b also shows that the Fe-(Ba-BC) samples are mostly composed of elemental C and O. Mn and K are present in the Fe-(Ba-BC) samples after alteration, whereas there are decreased amounts of elemental C and increased amounts of elemental O (Wang et al., 2020).

3.2. Competitive removal of SO_4^{2-} from modified and unmodified biochar samples

The effectiveness of different biochars with and without the addition of Ba^{2+} and impregnated with iron oxide (SDF, SD1, SD2, BBF1,

BBF2, BBC, BBR1, BBR2, BBS1 and BBS2) was examined and the adsorbent with the highest efficiency for the removal of SO_4^{2-} was selected for further evaluation. The experiment was carried out with a 1500 mg L^{-1} solution of SO_4^{2-} at pH 5.70 for a reaction time of 24 h using 0.1 M $BaCl_2$ and 0.5 g dose of the adsorbent at room temperature (22 ± 2 °C). The Ba^{2+}-loaded biochar sample SD1 showed the highest removal efficiency (Fig. 3a). The Ba^{2+} from $BaCl_2$ reacted with the SO_4^{2-} ion from Na_2SO_4 to give a white precipitate of $BaSO_4$ (Kartic et al., 2018). The impregnation of Fe on the surface of the biochar increased the surface area, resulting in a higher removal efficiency.

3.3. Effect of initial concentration of $BaCl_2$

The effect of the initial $BaCl_2$ concentration (0.05–0.25 M) on the removal of SO_4^{2-} was evaluated with an initial SO_4^{2-} concentration of 1500 mg L^{-1} at pH 5.7 with a dose of Fe-(Ba-BC) 0.5 g and a reaction time of 24 h. The highest concentration of 0.25 M $BaCl_2$ gave the highest removal efficiency for SO_4^{2-} of 78.2% (Fig. 3b), whereas the lower concentrations of $BaCl_2$ (0.05 and 0.1 M) only removed 18.2 and 20.3%, respectively, of the SO_4^{2-}. The Fe-(Ba-BC) sample dramatically increased the adsorption of pollutants (Ambaye et al., 2021) compared with unmodified biochar.

3.4. Effect of contact time

Precipitation-assisted adsorption processes were used to determine the effect of the contact time on the removal of SO_4^{2-} using a 1500 mg L^{-1} solution of SO_4^{2-}, 0.25 M $BaCl_2$ and 0.5 g of Fe-(Ba-BC) at pH 5.21 for reaction times of 0–510 min at ambient temperature. The removal efficiency increased rapidly from 30 to 480 min and then slowed down, reaching equilibrium after 480 min (Fig. 3c). The high rate of precipitation in the initial stages was a result of the availability of sorption sites on the surface of biochar. An increase in contact time did not affect the equilibrium and 96.5% of the SO_4^{2-} was removed. This indicates that the adsorption-assisted precipitation reached equilibrium, as reported previously by (Ali et al., 2018).

3.5. Effect of pH

The effect of pH (from pH 2 to 11) was investigated using a 1500 mg L^{-1} solution of SO_4^{2-}, 0.5 g of adsorbent, a 0.25 M solution of Ba^{2+} and a reaction time of 480 min at room temperature. The initial pH of the solutions influenced the initial concentration of SO_4^{2-}. The addition of Fe-(Ba-BC) for 480 min resulted in the removal of 99.385% of the SO_4^{2-} at pH 9 (Fig. 4a). Several studies have observed a significant role of pH (Kołodyńska et al., 2012). Both the surface charge and ionization of Fe-(Ba-BC) are dependent on pH and can be used to differentiate the adsorption efficiency for the removal of contaminants. A rapid decrease in the removal of SO_4^{2-} at low pH values was observed as a result of hydrolysis and ionization of the weak acid, which converted SO_4^{2-} to $BaSO_4$ (Agarwal and Balomajumder, 2015). The highest percentage removal of SO_4^{2-} was observed at alkaline pH values as a result of the strong electrostatic attraction between the $SO_4^{2-}$and the positively charged $BaCl_2$. These results showed that the electrostatic force of attraction is not the primary driver for the removal of SO_4^{2-} from wastewater, which takes place as a result of the surface coordination of the FeOH group. SO_4^{2-} was adsorbed via an ion-exchange mechanism. However, the alkaline pH in this study meant that OH^- predominated and competed with the other ions in the aqueous solution to bind to the $BaCl_2$ surface (Shah et al., 2021).

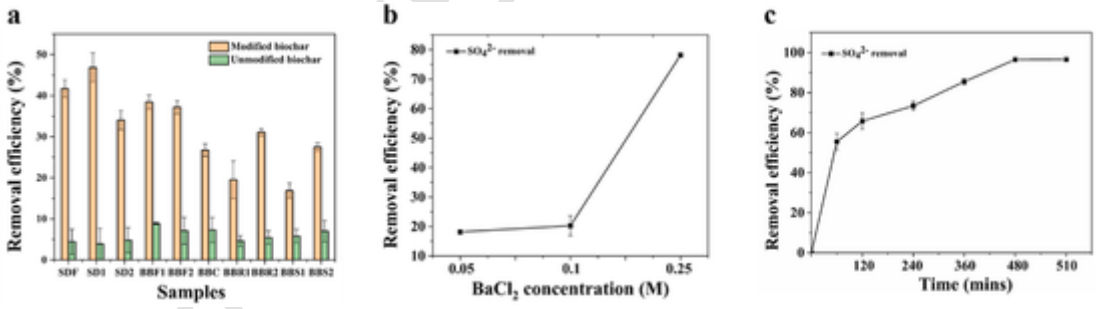

Fig. 3. Efficient SO_4^{2-} removal from aqueous solution with standard deviation. (**a**) Percentage removal of 1500 mg L^{-1} SO_4^{2-} using modified and unmodified biochar at room temperature. Fe-(Ba-BC) (SD1) shows maximum efficiency; (**b**) Increasing trend of SO_4^{2-} removal efficiency from Fe-impregnated biochar modified with $BaCl_2$ at room temperature; (**c**) Effect of retention time on removing SO_4^{2-} from Fe-impregnated biochar modified with $BaCl_2$ under optimum conditions.

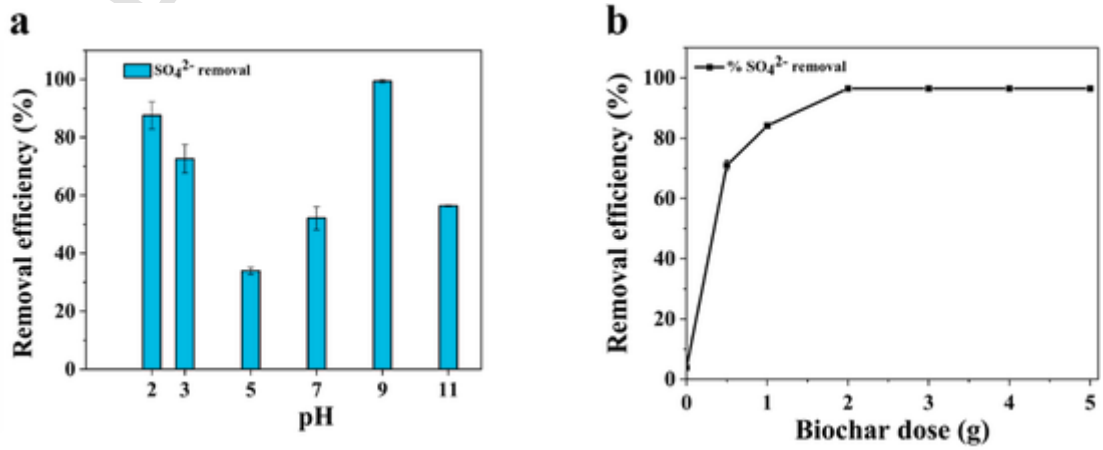

Fig. 4. (**a**) Effect of pH for removing SO_4^{2-} using Fe-impregnated biochar modified with $BaCl_2$ under optimum conditions; (**b**) Effect of adsorbent dose on SO_4^{2-} removal from Fe-impregnated biochar modified with $BaCl_2$ ($BaCl_2$ 0.25 M; contact time 480 min, pH 9) at room temperature.

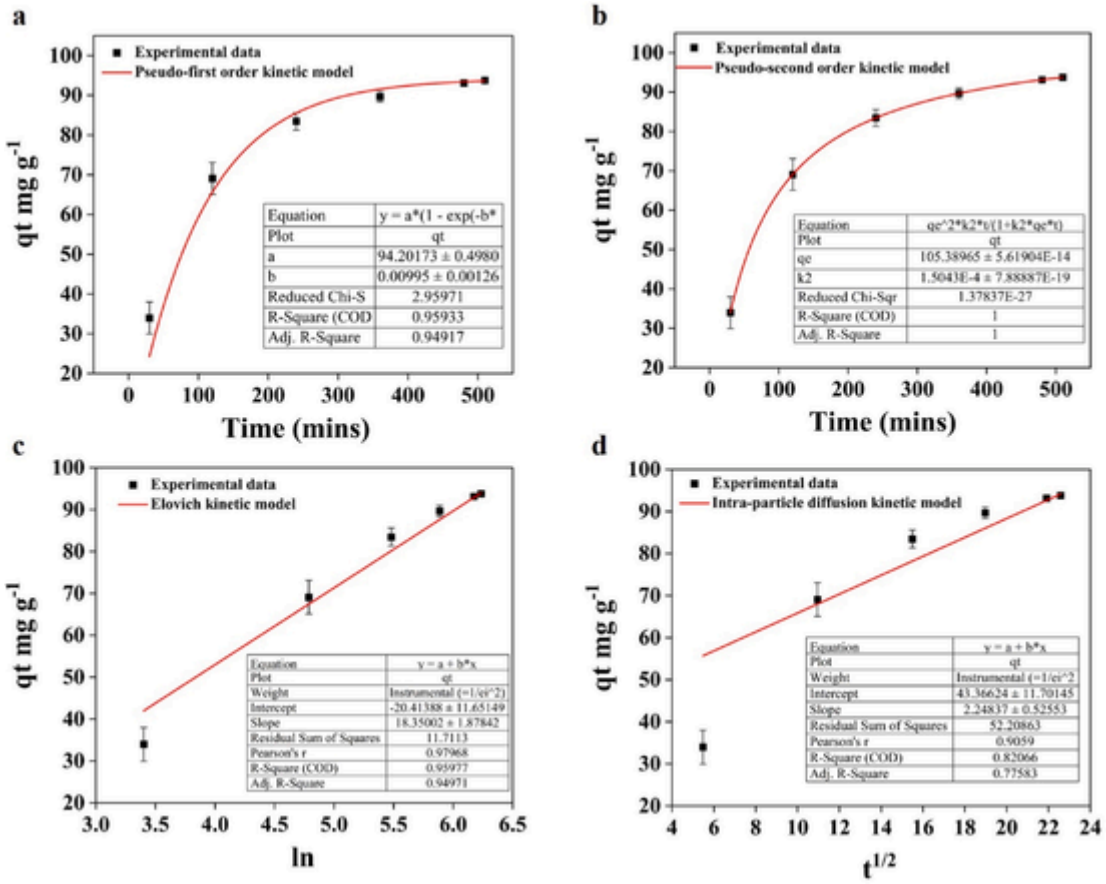

Fig. 5. Comparison of different models of sorption kinetics for removing SO_4^{2-} from Fe-impregnated biochar modified with $BaCl_2$ under optimum conditions. (**a**) Pseudo-first order; (**b**) Pseudo-second order; (**c**) Elovich equation; (**d**) Intraparticle diffusion using Fe-(Ba-BC) at optimal conditions, respectively. The data were fitted to PSO model.

3.6. Effect of adsorbent dose

The effect of adsorbent dose (0.5–5 g) on the removal of SO_4^{2-} was investigated under the optimum conditions (initial SO_4^{2-} concentration 1500 mg L^{-1}, pH 9, 0.25 M barium, reaction time 480 min at room temperature). The highest removal efficiency of SO_4^{2-} was 96.7% at an adsorbent dose of 2 g (Fig. 4b). The proportion of SO_4^{2-} removed via precipitation-assisted adsorption increased when the Fe-(Ba-BC) adsorbent dose increased. Many sorption sites were found on the surface of the Fe-(Ba-BC) samples. Equilibrium was established at a reaction time of 480 min. An increase in the dose of adsorbent up to 5 g did not influence the removal efficacy. An increase in the amount of Fe-(Ba-BC) increased the removal efficacy when the SO_4^{2-} concentration was decreased from 1500 to 226.8 mg L^{-1}. It was concluded that when Fe-(Ba-BC) was introduced for an extended period of time, the adsorption sites became supersaturated. This means that the amount of SO_4^{2-} adsorbed decreased and the removal rate reached a maximum (Ali et al., 2018).

3.7. Adsorption kinetics models

The rate of adsorption of SO_4^{2-} onto the surface of the Fe-(Ba-BC) samples was determined using the pseudo-first-order and PSO models (Miyake et al., 2013), the Elovich equation and the intraparticle diffusion model (Acevedo et al., 2015) (Fig. 5). The PSO rate equation (Fig. 5b) gave the best fit with a correlation coefficient of $R^2 = 1$. The PSO kinetic model assumes that chemisorption is the rate-limiting process and governs the adsorption of SO_4^{2-} via the exchange of electrons between Fe-(Ba-BC) and SO_4^{2-}. Fig. 5 shows that the PSO model, the Elovich equation and the intraparticle diffusion model all gave poor fits to the experimental data, suggesting that the rate-limiting step was chemical rather than physical adsorption. The PFO model (Fig. 5a), the intraparticle diffusion model (Fig. 5c) and the Elovich equation (Fig. 5d) gave coefficients of correlation of $R^2 = 0.99154$, 0.9059 and 0.97968, respectively. The PSO model applies to the adsorption method and shows the competitive adsorption of inorganic pollutants, which can be used to precipitate inorganic anions such as SO_4^{2-}. Hence the PSO model is superior to the other models (Shah et al., 2021; Tan and Hameed, 2017) and indicates that SO_4^{2-} was removed by the Fe-(Ba-BC) sample via chemisorption.

3.8. Removal mechanism

Many C-based materials have been modified to enhance the selective adsorption of metals via physical, chemical and metallic impregnation methods. Magnetic biochar can also be formed by incinerating biomass and impregnating it with iron oxides (Marchisio et al., 2002; Merdhah and Yassin, 2009). $BaCl_2$ behaves as a simple salt in an aqueous environment and is a 1:2 electrolyte in water, forming a solution with a neutral pH. In this study, the Ba^{2+} from $BaCl_2$ reacted with SO_4^{2-} ions from Na_2SO_4 to form an insoluble white precipitate of $BaSO_4$ and a solution of NaCl. The Fe-(Ba-BC) adsorbent provided a surface for the chemisorption of Ba^{2+}, with valency forces sharing electrons between the biochar and $BaCl_2$. The reaction of the Fe-(Ba-BC) sample with an aqueous solution of Na_2SO_4 resulted in a double displacement reaction because they exchanged ions or bonds to form new compounds (Fig. 6):

$$Ba^{2+}{}_{(s)} + SO_4{}^{2-}{}_{(aq)} \Rightarrow BaSO_{4(s)} \quad (8)$$

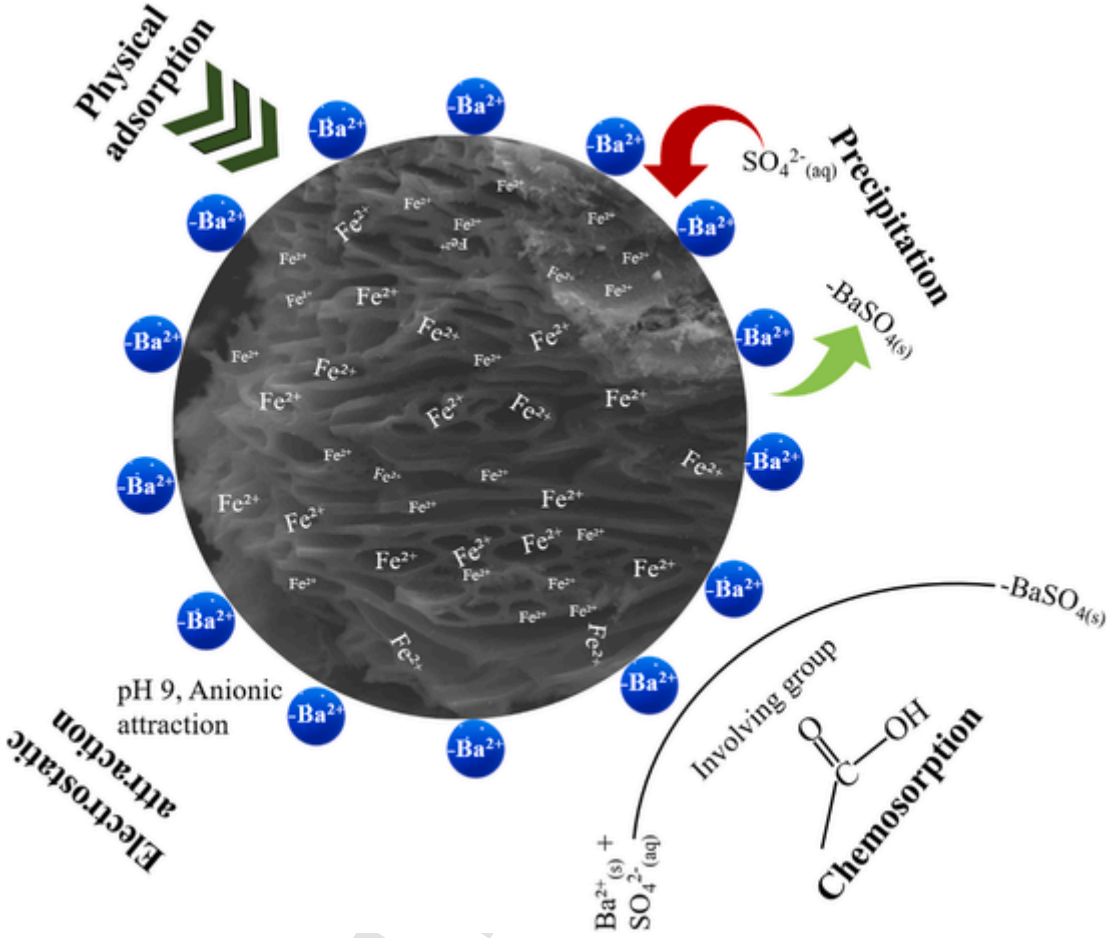

Fig. 6. Proposed mechanism of SO_4^{2-} removal by chemosorption from Fe-impregnated biochar modified with $BaCl_2$.

It has been shown previously that temperature has no significant effect on the precipitation of $BaSO_4$ (Kartic et al., 2018).

4. Conclusion

Fe-(Ba-BC) proved to be an efficient sorbent for the removal of SO_4^{2-} from aqueous solutions. The maximum removal efficiency achieved was 96.7% in 480 min at pH 9, 2 g of adsorbent, a 0.25 M solution of $BaCl_2$ and a fixed initial concentration of 1500 mg L^{-1} SO_4^{2-} at room temperature. The Raman analysis, including D and G bands, showed the high intensity of Fe-(Ba-BC) peaks before the experiment compared to after the experiment, indicating the reaction of $BaSO_4$ precipitation. The XRD, SEM, and EDS results confirm the modification of $BaCl_2$ onto the Fe-(Ba-BC). XRD is indicating the highest peak reflection $2\theta = 5.73^{\circ}$ while after experiment shows thriving reflections of $BaSO_4$ revealing the highest reflection $2\theta = 4.45^{\circ}$. SEM and EDS before the investigation shows weight percent of Ba 19.46% and 13.278. The results after the experiment show the decline peaks of Ba with weight 0.14% and 0.93% indicated the precipitation of $-Ba^{2+}$ combined with SO_4^{-2}. PSO kinetics with $R^2 = 1$ indicated chemosorption. These results confirm that Fe-(Ba-BC) could be used as an adsorbent to remove SO_4^{2-} from wastewater.

Credit authorship contribution statement

Warda Khalid: Conceptualization, Methodology, Data curation, Writing –original draft. **Chin Kui Cheng:** Review & editing. **Peng Liu:** Conceptualization, Supervision, Funding acquisition, Writing - review & editing, Project administration. **Jinping Tang:** Conceptualization, Methodology. **Xin Liu:** Conceptualization, Methodology. **Asmat Ali:** Conceptualization, Methodology, review & editing. **Asfandyar Shahab:** Review & editing. **Xingjie Wang:** Conceptualization, review & editing.

Declaration of competing interest

The authors declare that they have no known competing financial interests or personal relationships that could have appeared to influence the work reported in this paper.

Acknowledgments

This work was supported by the National Natural Science Foundation of China [grant number 41877478], and the Fundamental Research Funds for the Central Universities (China University of Geosciences (Wuhan) [grant number CUGGC06]).

References

Acevedo, B., Barriocanal, C., Lupul, I., Gryglewicz, G., 2015. Properties and performance of mesoporous activated carbons from scrap tyres, bituminous wastes and coal. Fuel 151, 83–90. https://doi/10.1016/j.fuel.2015.01.010.

Agarwal, B., Balomajumder, C., 2015. Removal of phenol and cyanide in multi-substrate system using copper impregnated activated carbon (Cu-GAC). Environ. Prog. Sustain. Energy 34 (6), 1714–1723. https://doi.org/10.1002/ep.12177.

Al-Zoubi, H., Hilal, N., Darwish, N., Mohammad, A., 2007. Rejection and modelling of sulphate and potassium salts by nanofiltration membranes: neural network and Spiegler–Kedem model. Desalination 206 (1–3), 42–60. https://doi/10.1016/j.desal.2006.02.060.

Ali, A., Bilal, M., Khan, R., Farooq, R., Siddique, M., 2018. Ultrasound-assisted adsorption of phenol from aqueous solution by using spent black tea leaves. Environ. Sci. Pollut. Res. 25 (23), 22920–22930. https://doi.org/10.1007/s11356-018-2186-9.

Alvarez, J., Lopez, G., Amutio, M., Bilbao, J., Olazar, M., 2015. Physical activation of rice husk pyrolysis char for the production of high surface area activated carbons. Ind. Eng. Chem. Res. 54 (29), 7241–7250. https://doi.org/10.1021/acs.iecr.5b01589.

Ambaye, T., Vaccari, M., van Hullebusch, E.D., Amrane, A., Rtimi, S., 2021. Mechanisms and adsorption capacities of biochar for the removal of organic and inorganic pollutants from industrial wastewater. Int. J. Environ. Sci. Technol. 18 (10), 3273–3294. https://doi.org/10.1007/s13762-020-03060-w.

Ao, H., Cao, W., Hong, Y., Wu, J., Wei, L., 2020. Adsorption of sulfate ion from water by zirconium oxide-modified biochar derived from pomelo peel. Sci. Total Environ. 708, 135092. https://doi.org/10.1016/j.scitotenv.2019.135092.

Asadullah, M., Zhang, S., Min, Z., Yimsiri, P., Li, C.-Z., 2010. Effects of biomass char structure on its gasification reactivity. Bioresour. Technol. 101 (20), 7935–7943. https://doi.org/10.1016/j.biortech.2010.05.048.

Bashir, M.T., Ali, S., Bashir, A., 2012. Health effects from exposure to sulphates and chlorides in drinking water. Pakistan J. Med. Health Sci. 3, 648–652.

Chen, B., Chen, Z., Lv, S., 2011. A novel magnetic biochar efficiently sorbs organic pollutants and phosphate. Bioresour. Technol. 102 (2), 716–723. https://doi.org/10.1016/j.biortech.2010.08.067.

Chen, X., Zheng, L., Dong, X., Jiang, C., Wei, X., 2020. Sources and mixing of sulfate contamination in the water environment of a typical coal mining city, China: evidence from stable isotope characteristics. Environ. Geochem. Health 42 (9), 2865–2879. https://doi.org/10.1007/s10653-020-00525-2.

Cheng, Z., Gao, Z., Ma, W., Sun, Q., Wang, B., Wang, X., 2012. Preparation of magnetic Fe3O4 particles modified sawdust as the adsorbent to remove strontium ions. Chem. Eng. J. 209, 451–457. https://doi.org/10.1016/j.cej.2012.07.078.

Duan, X., Zhang, C., Srinivasakannan, C., Wang, X., 2017. Waste walnut shell valorization to iron loaded biochar and its application to arsenic removal. Resour. Efficient.Technol. 3 (1), 29–36. https://doi.org/10.1016/j.reffit.2017.01.001.

Dutta, P.K., Rabaey, K., Yuan, Z., Rozendal, R.A., Keller, J., 2010. Electrochemical sulfide removal and recovery from paper mill anaerobic treatment effluent. Water Res. 44 (8), 2563–2571. https://doi.org/10.1016/j.watres.2010.01.008.

EPA, U., 2017. Secondary Drinking Water Standards: Guidance for Nuisance Chemicals. Drinking Water Contaminants-Standards and Regulations. US EPA, Publisher. https://www.epa.gov/sdwa/secondary-drinking-water-standards-guidance-nuisance-chemicals.

Feng, D., Zhao, Y., Zhang, Y., Sun, S., Meng, S., Guo, Y., Huang, Y., 2016. Effects of K and Ca on reforming of model tar compounds with pyrolysis biochars under H2O or CO2. Chem. Eng. J. 306, 422–432. https://doi.org/10.1016/j.cej.2016.07.065.

Feng, G., Ma, J., Zhang, X., Zhang, Q., Xiao, Y., Ma, Q., Wang, S., 2019. Magnetic natural composite Fe3O4-chitosan@ bentonite for removal of heavy metals from acid mine drainage. J. Colloid Interface Sci. 538, 132–141. https://doi.org/10.1016/j.jcis.2018.11.087.

Gillingham, M.D., Gomes, R.L., Ferrari, R., West, H.M., 2021. Sorption, separation and recycling of ammonium in agricultural soils: a viable application for magnetic biochar? Sci. Total Environ. 151440. https://doi.org/10.1016/j.scitotenv.2021.151440.

Ho, Y.-S., McKay, G., 1998. Sorption of dye from aqueous solution by peat. Chem. Eng. J. 70 (2), 115–124. https://doi.org/10.1016/S0923-0467(98)00076-1.

Hudaib, B., 2021. Treatment of real industrial wastewater with high sulfate concentrations using modified Jordanian kaolin sorbent: batch and modelling studies. Heliyon 7 (11), e08351. https://doi.org/10.1016/j.heliyon.2021.e08351.

Kartic, D.N., Narayana, B.C.A., Arivazhagan, M., 2018. Removal of high concentration of sulfate from pigment industry effluent by chemical precipitation using barium chloride: RSM and ANN modeling approach. J. Environ. Manag. 206, 69–76. https://doi.org/10.1016/j.jenvman.2017.10.017.

Kołodyńska, D., Wnętrzak, R., Leahy, J., Hayes, M., Kwapiński, W., Hubicki, Z., 2012. Kinetic and adsorptive characterization of biochar in metal ions removal. Chem. Eng. J. 197, 295–305. https://doi.org/10.1016/j.cej.2012.05.025.

Lagergren, S.K., 1898. About the theory of so-called adsorption of soluble substances. Sven. Vetenskapsakad. Handingarl 24, 1–39.

Li, H., Zhang, D., Han, X., Xing, B., 2014. Adsorption of antibiotic ciprofloxacin on carbon nanotubes: pH dependence and thermodynamics. Chemosphere 95, 150–155. https://doi.org/10.1016/j.chemosphere.2013.08.053.

Li, M., Ren, L., Zhang, J., Luo, L., Qin, P., Zhou, Y., Huang, C., Tang, J., Huang, H., Chen, A., 2019. Population characteristics and influential factors of nitrogen cycling functional genes in heavy metal contaminated soil remediated by biochar and compost. Sci. Total Environ. 651, 2166–2174. https://doi.org/10.1016/j.scitotenv.2018.10.152.

Li, X., Jia, Y., Zhou, M., Su, X., Sun, J., 2020. High-efficiency degradation of organic pollutants with Fe, N co-doped biochar catalysts via persulfate activation. J. Hazard Mater. 397, 122764. https://doi.org/10.1016/j.jhazmat.2020.122764.

Liang, L., Xi, F., Tan, W., Meng, X., Hu, B., Wang, X., 2021. Review of organic and inorganic pollutants removal by biochar and biochar-based composites. Biochar 3 (3), 255–281. https://doi.org/10.1007/s42773-021-00101-6.

Lu, Z., Zhang, H., Shahab, A., Zhang, K., Zeng, H., Nabi, I., Ullah, H., 2021. Comparative study on characterization and adsorption properties of phosphoric acid activated biochar and nitrogen-containing modified biochar employing Eucalyptus as a precursor. J. Clean. Prod. 303, 127046. https://doi.org/10.1016/j.jclepro.2021.127046.

Marchisio, D., Barresi, A., Garbero, M., Vanni, M., Baldi, G., 2002. Study of aggregation in barium sulphate precipitation. In: Proceedings of the 15 Th International Symposium on Industrial Crystallization. pp. 15–18.

Merdhah, A.B.B., Yassin, A.A.M., 2009. Laboratory study on precipitation of barium sulphate in Malaysia sandstone cores. Petrol. Eng. J. 2 (1). https://doi.org/10.2174/1874834101002010001.

Miyake, Y., Ishida, H., Tanaka, S., Kolev, S.D., 2013. Theoretical analysis of the pseudo-second order kinetic model of adsorption. Application to the adsorption of Ag (I) to mesoporous silica microspheres functionalized with thiol groups. Chem. Eng. J. 218, 350–357. http://doi:10.1016/J.CEJ.2012.11.089.

Mo, Z., Shi, Q., Zeng, H., Lu, Z., Bi, J., Zhang, H., Rinklebe, J., Lima, E.C., Rashid, A., Shahab, A., 2021. Efficient removal of Cd (II) from aqueous environment by potassium permanganate-modified eucalyptus biochar. Biomass Convers. Biorefin. 1–13. https://doi.org/10.1007/s13399-021-02126-0.

Mo, Z., Tai, D., Zhang, H., Shahab, A., 2022. A comprehensive review on the adsorption of heavy metals by zeolite imidazole framework (ZIF-8) based nanocomposite in water. Chem. Eng. J. 136320. https://doi.org/10.1016/j.cej.2022.136320.

Mohammadi, M., Mowla, D., Esmaeilzadeh, F., Ghasemi, Y., 2019. Enhancement of sulfate removal from the power plant wastewater using cultivation of indigenous microalgae: stage-wise operation. Chem. Eng. 7 (1), 102870. https://doi.org/10.1016/j.jece.2018.102870.

Mulinari, D.R., da Silva, M.L.C., 2008. Adsorption of sulphate ions by modification of sugarcane bagasse cellulose. Carbohydr. Polym. 74 (3), 617–620. https://doi.org/10.1016/j.carbpol.2008.04.014.

Park, S., Baker, J.O., Himmel, M.E., Parilla, P.A., Johnson, D.K., 2010. Cellulose crystallinity index: measurement techniques and their impact on interpreting cellulase performance. Biotechnol. Biofuels 3 (1), 1–10. https://doi.org/10.1186/1754-6834-3-10.

Rajapaksha, A.U., Chen, S.S., Tsang, D.C., Zhang, M., Vithanage, M., Mandal, S., Gao, B., Bolan, N.S., Ok, Y.S., 2016. Engineered/designer biochar for contaminant removal/immobilization from soil and water: potential and implication of biochar modification. Chemosphere 148, 276–291. https://doi.org/10.1016/j.chemosphere.2016.01.043.

Rodrigues, C., Follmann, H.V., Núñez-Gómez, D., Nagel-Hassemer, M.E., Lapolli, F.R., Lobo-Recio, M.Á., 2020. Sulfate removal from mine-impacted water by electrocoagulation: statistical study, factorial design, and kinetics. Environ. Sci. Pollut. Res. 27 (31), 39572–39583. https://doi.org/10.1007/s11356-020-09758-1.

Runtti, H., Tuomikoski, S., Kangas, T., Kuokkanen, T., Rämö, J., Lassi, U., 2016. Sulphate removal from water by carbon residue from biomass gasification: effect of chemical modification methods on sulphate removal efficiency. Bio 11 (2), 3136–3152.

Shah, I.A., Ali, S., Khan, M.T., Qureshi, M.B.A., Shah, S.H.A., Ali, A., Rashid, W., Gul, H.N., 2021. Synthesis and evaluation of Ca-doped ferrihydrite as A novel adsorbent for the efficient removal of fluoride. Environ. Sci. Pollut. Res. 29, 6375–6388. https://doi.org/10.1007/s11356-021-16105-5.

Silva, A.F.R., Magalhães, N.C., Cunha, P.V.M., Amaral, M.C.S., Koch, K., 2020. Influence of COD/SO42− ratio on vinasse treatment performance by two-stage anaerobic membrane bioreactor. J. Environ. Manag. 259, 110034. https://doi.org/10.1016/j.jenvman.2019.110034.

Srivatsav, P., Bhargav, B.S., Shanmugasundaram, V., Arun, J., Gopinath, K.P., Bhatnagar, A., 2020. Biochar as an eco-friendly and economical adsorbent for the removal of colorants (dyes) from aqueous environment: a review. Water 12 (12), 3561. https://doi.org/10.3390/w12123561.

Sun, Y., Liu, Z., Fei, Z., Li, C., Chun, Y., Zhang, A., 2019. Synergistic effect and degradation mechanism on Fe-Ni/CNTs for removal of 2, 4-dichlorophenol in aqueous solution. Environ. Sci. Pollut. Res. 26 (9), 8768–8778. https://doi.org/10.1007/s11356-019-04394-w.

Tan, K., Hameed, B., 2017. Insight into the adsorption kinetics models for the removal of contaminants from aqueous solutions. J. Taiwan Inst. Chem. Eng. 74, 25–48. https://doi.org/10.1016/j.jtice.2017.01.024.

Tang, W., He, D., Zhang, C., Waite, T.D., 2017. Optimization of sulfate removal from brackish water by membrane capacitive deionization (MCDI). Water Res. 121, 302–310. https://doi.org/10.1016/j.fuel.2011.02.044.

Tay, H.-L., Kajitani, S., Zhang, S., Li, C.-Z., 2013. Effects of gasifying agent on the evolution of char structure during the gasification of Victorian brown coal. Fuel 103, 22–28. https://doi.org/10.1016/j.fuel.2011.02.044.

Wang, J., Cai, J., Wang, S., Zhou, X., Ding, X., Ali, J., Zheng, L., Wang, S., Yang, L., Xi, S., 2022. Biochar-based activation of peroxide: multivariate-controlled performance, modulatory surface reactive sites and tunable oxidative species. Chem. Eng. J. 428, 131233. https://doi.org/10.1016/j.cej.2021.131233.

Wang, J., Chen, C., 2014. Chitosan-based biosorbents: modification and application for biosorption of heavy metals and radionuclides. Bioresour. Technol. 160, 129–141. https://doi.org/10.1016/j.biortech.2013.12.110.

Wang, W., Zhang, J., Chen, T., Sun, J., Ma, X., Wang, Y., Wang, J., Xie, Z., 2020. Preparation of TiO 2-modified biochar and its characteristics of photo-catalysis degradation for enrofloxacin. Sci. Rep. 10 (1), 1–12. https://doi.org/10.1038/s41598-020-62791-5.

Water, S., Organization, W.H., 2006. Guidelines for Drinking-Water Quality: Incorporating First Addendum, vol. 1. Recommendations.

Yi, Z., Liu, J., Zeng, R., Liu, X., Long, J., Huang, B., 2020. Removal of uranium (VI) from aqueous solution by Camellia oleifera shell-based activated carbon: adsorption equilibrium, kinetics, and thermodynamics. Water Sci. Technol. 82 (11), 2592–2602. https://doi.org/10.2166/wst.2020.504.

Zak, D., Hupfer, M., Cabezas, A., Jurasinski, G., Audet, J., Kleeberg, A., McInnes, R., Kristiansen, S.M., Petersen, R.J., Liu, H., 2021. Sulphate in freshwater ecosystems: a review of sources, biogeochemical cycles, ecotoxicological effects and bioremediation. Earth Sci. Rev. 212, 103446. https://doi.org/10.1016/j.earscirev.2020.103446.

Zeldowitsch, J., 1934. Über den mechanismus der katalytischen oxydation von CO an MnO_2. Acta physicochim. URSS 1, 364–449.

Zeng, H., Zeng, H., Zhang, H., Shahab, A., Zhang, K., Lu, Y., Nabi, I., Naseem, F., Ullah, H., 2021. Efficient adsorption of Cr (VI) from aqueous environments by phosphoric acid activated eucalyptus biochar. J. Clean. Prod. 286, 124964. https://doi.org/10.1016/j.jclepro.2020.124964.

Zhang, J., Wang, Y., Zhang, L., Zhang, R., Liu, G., Cheng, G., 2014. Understanding changes in cellulose crystalline structure of lignocellulosic biomass during ionic liquid pretreatment by XRD. Bioresour. Technol. 151, 402–405. https://doi.org/10.1016/j.biortech.2013.10.009.

Zheng, T., Dahn, J., 1999. Applications of carbon in lithium-ion batteries. Carbon Mater. Adv. Technol. 341–388.